

OTFS-NOMA based on SCMA

Kuntal Deka¹, Anna Thomas¹, and Sanjeev Sharma²

¹Indian Institute of Technology Goa, India, ²Indian Institute of Technology (BHU) Varanasi, India

Abstract—Orthogonal Time Frequency Space (OTFS) is a 2-D modulation technique that has the potential to overcome the challenges faced by orthogonal frequency division multiplexing (OFDM) in high Doppler environments. The performance of OTFS in a multi-user scenario with orthogonal multiple access (OMA) techniques has been impressive. Due to the requirement of massive connectivity in 5G and beyond, it is immensely essential to devise and examine the OTFS system with the existing Non-orthogonal Multiple Access (NOMA) techniques. In this paper, we propose a multi-user OTFS system based on a code-domain NOMA technique called Sparse Code Multiple Access (SCMA). This system is referred to as the OTFS-SCMA model. The framework for OTFS-SCMA is designed for both downlink and uplink. First, the sparse SCMA codewords are strategically placed on the delay-Doppler plane such that the overall overloading factor of the OTFS-SCMA system is equal to that of the underlying basic SCMA system. The receiver in downlink performs the detection in two sequential phases: first, the conventional OTFS detection using the method of linear minimum mean square error (LMMSE), and then the conventional SCMA detection. For uplink, we propose a single-phase detector based on message-passing algorithm (MPA) to detect the multiple users' symbols. The performance of the proposed OTFS-SCMA system is validated through extensive simulations both in downlink and uplink. We consider delay-Doppler planes of different parameters and various SCMA systems of overloading factor up to 200%. The performance of OTFS-SCMA is compared with those of existing OTFS-OMA techniques. The comprehensive investigation demonstrates the usefulness of OTFS-SCMA in future wireless communication standards.

Index Terms—OTFS, SCMA, NOMA, message passing algorithm.

I. INTRODUCTION

Orthogonal Time Frequency Space (OTFS) has emerged as a promising modulation technique that eliminates the shortcomings of orthogonal frequency division multiplexing (OFDM) in 5G [1, 2]. Many applications facilitated by 5G involve vehicle-to-vehicle and vehicle-to-infrastructure communication scenario with the presence of high-speed vehicles. OFDM is not robust to such high Doppler environments as the sub-carriers don't remain orthogonal.

OTFS modulation technique succeeds in such cases by operating in the delay-Doppler domain instead of the conventional time-frequency domain. By representing the channel in delay-Doppler domain, it is possible to convert the time-variant channel response $h(\tau, t)$ to time-invariant channel response $h(\tau, \nu)$ where, t, τ and ν represent time, delay and Doppler respectively. This representation directly describes the geometrical features of a channel. As the reflecting objects move slowly, the time-variation of the delay-Doppler channel representation is minimal. Apart from the channel representation, the most distinguishing feature of the OTFS modulation is that the

information symbols are directly put in the delay-Doppler grid. The OTFS modulation principle is inspired by the existence of 2-D orthogonal signals in delay-Doppler domain where they behave as simultaneously localized in both time and frequency. An information symbol placed on a delay-Doppler grid spans the entire allotted time-frequency plane using these orthogonal basis functions. Thus irrespective of the position of symbol in the delay-Doppler grid, all of the symbols with the same power will experience the same channel. This invariance property provides OTFS its remarkable performance compared to existing modulation techniques especially in high Doppler channel conditions [1, 3].

Non-orthogonal multiple access (NOMA) is a popular multiple access framework particularly suited for applications involving massive connectivity [4]. The NOMA schemes can be divided into two domains: *power domain* and *code-domain*. In power-domain NOMA, different users are identified using different levels of the assigned power [5]. In code-domain NOMA, the multiple users are distinguished using different codewords assigned to them [6]. Sparse Code Multiple Access (SCMA) is a code-domain NOMA technique where sparse codewords are assigned to the users' symbols [7]. The sparsity of the codewords facilitates the successful use of the message passing algorithm (MPA) [8] for the detection of the users' symbols.

Related work: The study of multiple access technologies in the OTFS framework is an important topic. The authors in [9] proposed an OTFS-OMA scheme such that the multiple users' symbols are spread at equal interval over the entire delay-Doppler plane. These symbols are restricted to non-overlapping contiguous sub-blocks in the time-frequency plane. An OTFS-OMA scheme is presented in [10] where the multiple users' symbols are put in non-overlapping sub-blocks of the delay-Doppler plane. The OTFS-OMA method in [11] allocates interleaved symbols of different users in time-frequency domain. Note that here unlike [9], the allocation is not contiguous in the time-frequency plane, it is rather interleaved, i.e., between two symbols of one user, a symbol from another user can be put. The authors in [12] considered a power-domain NOMA system where the user with the highest velocity operates with OTFS and the remaining users operate with OFDM. In [13], power domain NOMA is considered with OTFS. Link level simulations of the coded OTFS-power domain NOMA system are presented for downlink and uplink.

Contributions: In this paper, we propose an OTFS-NOMA scheme based on a code-domain NOMA technique. The code-domain NOMA considered here is SCMA. Although OTFS-NOMA schemes have been studied in power-domain, to the

best of the authors' knowledge, this work is the first attempt to build an OTFS-NOMA system in the code-domain. First, we configure the OTFS-SCMA scheme in downlink. The SCMA codewords are sparse column vectors. We consider two schemes of allocating the SCMA codewords over the delay-Doppler plane. First scheme allocates the vector codewords in the vertical sub-columns in the Doppler direction. In the second scheme, the codewords are placed horizontally in the direction of delay bins. The detector in downlink is a two-phased process: (1) OTFS detector followed by (2) SCMA detector. The BER performances of this OTFS-SCMA method are evaluated for both the schemes with different sizes of delay-Doppler plane. It is observed that the codeword allocation scheme is not crucial. The BER performances are compared with those of existing conventional OTFS-OMA methods. In most of the cases, the OTFS-SCMA approach is found to provide better results than the existing OTFS-OMA. Next we devise the strategy of OTFS-SCMA in uplink. It turns out that the simple two-stage detection approach adopted in downlink is not applicable in uplink. A combined approach is considered to carry out OTFS and SCMA detection. An MPA detector is formulated to detect the multiple users' data at one go. The simulation results for different delay-Doppler planes are provided.

Outline: Section II describes the preliminaries such as OTFS modulation principle and input-output relations, SCMA system model and its related parameters. The proposed method of OTFS-SCMA is presented in Section III. The simulation results are presented and analyzed in Section IV. Section V concludes the paper.

Notations: \mathbb{C} denotes the set of all complex numbers. \mathbb{A} refers to the underlying alphabet for the symbols. Boldface uppers-case and boldface lower-case letters are used to denote the matrices and vectors respectively. I_N denotes the identity matrix of size $N \times N$. For a vector \mathbf{h} , $\text{diag}(\mathbf{h})$ is the diagonal matrix with the first diagonal being \mathbf{h} . The complex conjugation of x is denoted by x^* . For any integers k and N , the notation $[k]_N$ refers to $k \bmod N$.

II. PRELIMINARIES

A. OTFS

This section briefly explains the delay-Doppler symbol representation and the modulation-demodulation in OTFS. OTFS modulation technique introduced the idea of the allocation of symbols in delay-Doppler domain. In OTFS, the information symbols (e.g. QAM symbols) are arranged on a 2-D grid called delay-Doppler grid represented by $\Gamma_{M,N}$, where M and N correspond to the delay and Doppler dimension respectively. A total of MN QAM symbols can be transmitted on $\Gamma_{M,N}$. The input signal $x[k, l]$ refers to the symbol at k^{th} Doppler bin and l^{th} delay bin, where $k = 0, 1, \dots, N-1$ and $l = 0, 1, \dots, M-1$.

1) *Design parameters of delay-Doppler grid:* Consider a data transmission frame of duration $T_f = NT$ and bandwidth $B = M\Delta f$ such that $T = \frac{1}{\Delta f}$. The delay-Doppler grid has to be designed in such a way that $\tau_{\max} < \frac{1}{\Delta f}$ and

$\nu_{\max} < \frac{1}{T}$ where τ_{\max} and ν_{\max} are the delay and the Doppler spread respectively. Therefore $\Gamma_{M,N}$ has a delay interval of $\Delta\tau = \frac{1}{M\Delta f}$ and Doppler interval of $\Delta\nu = \frac{1}{NT}$. Hence to transmit NM symbols over a frame of duration T_f and bandwidth B , the choice of N and M depends on the delay and Doppler conditions of the channel. A channel with a high Doppler spread ν_{\max} would require a higher $N\Delta\nu$. It points to smaller T and larger Δf , which directly implies larger N and smaller M . Similarly if the channel has higher delay spread τ_{\max} , we require a higher $M\Delta\tau$ and the design of $\Gamma_{M,N}$ is to be done with a larger M and a smaller N [14].

The basic modulation-demodulation involved in an OTFS scheme is shown in Fig. 1. It includes two stages of modulation/demodulation, one in the delay-Doppler domain and the other in the time-frequency domain.

2) *Operations in Delay-Doppler Domain :* As we know, the QAM symbols ($x[k, l]$ s) to be transmitted are arranged in $\Gamma_{M,N}$ grid initially. The symbols ($y[k, l]$ s) finally received are also in $\Gamma_{M,N}$ grid. A 2-D transform pair known as Symplectic Finite Fourier Transform (SFFT) and Inverse Symplectic Finite Fourier Transform (ISFFT) is used in OTFS. SFFT is used for forward transformation from the time-frequency domain to the delay-Doppler domain and ISFFT is used for the reverse. It is noteworthy that SFFT (ISFFT too) is a combination of a forward Fourier transform and an inverse Fourier transform [3, 14]. At first the symbols in delay-Doppler domain are transformed into time-frequency domain using ISFFT as shown below:

$$X[n, m] = \frac{1}{NM} \sum_{k=0}^{N-1} \sum_{l=0}^{M-1} x[k, l] e^{j2\pi(\frac{nk}{N} - \frac{ml}{M})}. \quad (1)$$

Similarly at the receiver side, the signals received in the time-frequency domain are finally transformed back to the delay-Doppler domain using SFFT as described below:

$$y[k, l] = \sum_{n=0}^{N-1} \sum_{m=0}^{M-1} Y[n, m] e^{-j2\pi(\frac{nk}{N} - \frac{ml}{M})}. \quad (2)$$

Since the 2-D grid has to be limited to a dimension of $M \times N$, a rectangular windowing function is used both at the transmitter and the receiver side.

3) *Operations in Time-Frequency Domain :* The symbols $X[n, m]$ s look like inputs to regular OFDM data transmission. The only difference is that OTFS is a 2-D modulation technique while OFDM is 1-D modulation. An OTFS signal can be considered as a sequence of OFDM signals. The 2-D modulated signal in the time-frequency domain has to be converted to time-domain using a suitable transformation. Heisenberg transform deals with this transformation at the transmitter side using a basis pulse represented by $g_{\text{tx}}(t)$. Heisenberg's transform can be mathematically expressed as the modulation of $X[n, m]$ on $g_{\text{tx}}(t)$ as shown below:

$$s(t) = \sum_{n=0}^{N-1} \sum_{m=0}^{M-1} X[n, m] e^{j2\pi m \Delta f (t-nT)} g_{\text{tx}}(t-nT). \quad (3)$$

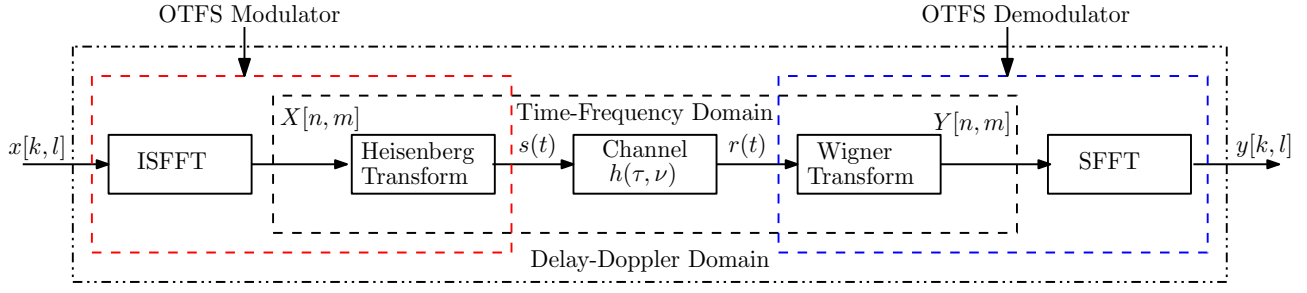


Fig. 1: OTFS Block Diagram.

The signal $s(t)$ is transmitted over the wireless channel with impulse response $h(\tau, \nu)$. The received signal $r(t)$ is given by

$$r(t) = \iint h(\tau, \nu) e^{j2\pi\nu(t-\tau)} s(t-\tau) d\tau d\nu + n(t) \quad (4)$$

where, $n(t)$ is the additive white Gaussian noise (AWGN) signal.

Similar to Heisenberg transform, there exists an inverse transform at the receiver side for transforming the time-domain signal back to the time-frequency plane. This inverse transform is known as Wigner transform which demodulates the received signal $r(t)$ to $Y[n, m]$. A suitably designed basis pulse $g_{rx}(t)$ is used in the received side.

For demodulation, the matched filter first computes the cross-ambiguity function $A_{g_{rx}, r}(\tau, \nu)$ between the received signal $r(t)$ and the receive pulse $g_{rx}(t)$. The cross-ambiguity function is a type of 2-D correlation function and is given by

$$A_{g_{rx}, r}(\tau, \nu) \triangleq \int e^{-j2\pi\nu(t-\tau)} g_{rx}^*(t-\tau) r(t) dt. \quad (5)$$

Sampling the matched filter output at regular intervals of $(nT, m\Delta f)$ gives the 2-D time-frequency demodulated signal $Y[n, m]$ as given below:

$$Y[n, m] = A_{g_{rx}, r}(\tau, \nu)|_{\tau=nT, \nu=m\Delta f}. \quad (6)$$

The selection of $g_{tx}(t)$ and $g_{rx}(t)$ is to be done wisely so that ideally they obey the bi-orthogonality property otherwise there will be interference from different delay and Doppler bins. The bi-orthogonality property can be written as given in the following:

$$\int e^{-j2\pi m\Delta f(t-nT)} g_{rx}^*(t-nT) g_{tx}(t) dt = \delta(m)\delta(n). \quad (7)$$

The pulses $g_{tx}(t)$ and $g_{rx}(t)$ which satisfy the bi-orthogonality property are known as *ideal* pulses. For the simple *rectangular* pulses, $g_{tx}(t)$ and $g_{rx}(t)$ have amplitude $1/\sqrt{T}$ for $t \in [0, T]$ and 0 at all other values. Note that the rectangular pulses don't satisfy the bi-orthogonality condition. The ideal pulses don't exist in real world. Therefore we focus on the rectangular pulses in the rest of the paper.

4) *Input-Output Relation*: The input-output relation refers to the relation between $x[k, l]$ s and $y[k, l]$ s. The input-output relation is helpful for designing detectors in the receiver side. The channel response in the delay-Doppler domain can be

sparingly represented as

$$h(\tau, \nu) = \sum_{i=1}^P h_i \delta(\tau - \tau_i) \delta(\nu - \nu_i) \quad (8)$$

where, P denotes the number of paths in the channel; h_i , τ_i and ν_i denote the i^{th} path's gain, delay and Doppler shift respectively. To conveniently express the input-output relation, the delay and Doppler taps for the i^{th} path can be alternatively represented as [14]

$$\tau_i = \frac{l_{\tau_i}}{M\Delta f}, \quad \nu_i = \frac{k_{\nu_i} + \kappa_{\nu_i}}{NT}$$

with some integers l_{τ_i}, k_{ν_i} and $\kappa_{\nu_i} \in [-0.5, 0.5]$ which represents fractional Doppler shift.

With the above sparse channel representation, the received signal $y[k, l]$ in the delay-Doppler domain for rectangular pulses is given by [14]

$$y[k, l] \approx \sum_{i=1}^P \sum_{q=-N_i}^{N_i} h_i e^{j2\pi \left(\frac{l-l_{\tau_i}}{M} \right) \left(\frac{k_{\nu_i} + \kappa_{\nu_i}}{N} \right)} \alpha_i(k, l, q) \times x[[k - k_{\nu_i} + q]_N, [l - l_{\tau_i}]_M] \quad (9)$$

where,

$$\alpha_i(k, l, q) = \begin{cases} \frac{1}{N} \beta_i(q) & l_{\tau_i} \leq l < M \\ \frac{1}{N} (\beta_i(q) - 1) e^{-j2\pi \frac{[k - k_{\nu_i} + q]_N}{N}} & 0 \leq l < l_{\tau_i} \\ \beta_i(q) = \frac{e^{-j2\pi(-q - \kappa_{\nu_i})} - 1}{e^{-j2\pi \frac{q}{N}(-q - \kappa_{\nu_i})} - 1}. \end{cases} \quad (10)$$

In (9) and (10), the number N_i appears when fractional Doppler shift exists. N_i denotes the number of neighboring Doppler points interfering with the particular point under consideration. Usually the value of N_i is significantly smaller than the total number N of Doppler bins. Observe that the AWGN term is omitted in (9) for compact description.

The input-output relation given in (9) can be represented by a set of linear equations of the following form [14]:

$$\mathbf{y} = \mathbf{H}\mathbf{x} + \mathbf{z} \quad (11)$$

where, $\mathbf{y} \in \mathbb{C}^{NM \times 1}$, $\mathbf{z} \in \mathbb{C}^{NM \times 1}$ and $\mathbf{x} \in \mathbb{A}^{NM \times 1}$ are the row-wise vectorized versions of the output, AWGN and the input respectively; $\mathbf{H} \in \mathbb{C}^{NM \times NM}$ is called as the coefficient matrix. A detailed explanation on formulating \mathbf{H}

matrix with any practical waveforms is given in [15]. This linear relationship is valid in the case of both ideal and practical pulse, though the elements of \mathbf{H} matrix change. The coefficient matrix \mathbf{H} has exactly $S = \sum_{i=1}^P (2N_i + 1)$ non-zero elements in each row and column. In absence of fractional Doppler shifts (i.e. $N_i = 0$), we have $S = P$. This makes \mathbf{H} matrix highly sparse. Owing to the sparsity of \mathbf{H} , the detection can be carried out with the help of MPA [10, 14, 16]. In place of MPA, other low-complexity linear equalization algorithms like LMMSE can also be effectively used by considering the block-circulant property of \mathbf{H} matrix [17, 18].

B. SCMA

SCMA is a highly sophisticated code-domain NOMA technique. A distinct codebook is assigned to each user such that no two users would have to use the same codeword. The basic parameters of SCMA and the other related concepts are briefly explained next.

1) *SCMA Parameters*: An SCMA system is represented as $J \times K$ model, where there are J users sharing K orthogonal resources. As $J > K$, we have an overloaded system with an overloading factor, $\lambda = \frac{J}{K} > 100\%$. As an example, the 6×4

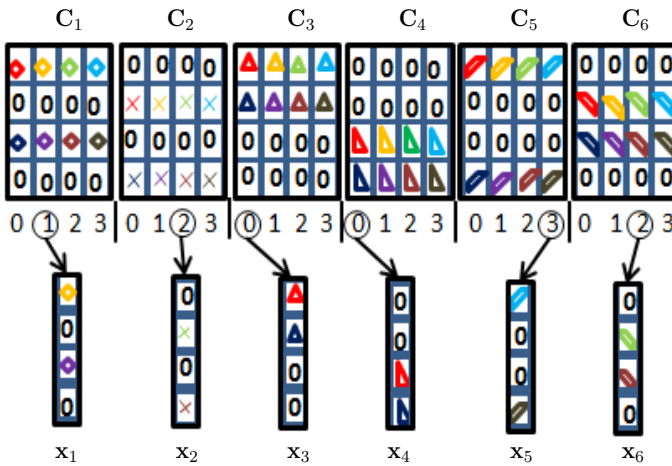


Fig. 2: Basic 6×4 SCMA Model.

SCMA system shown in Fig. 2 has 6 users sharing 4 resources with an overloading factor of 150%. The system has six distinct codebooks $\{C_1, C_2, \dots, C_6\}$ dedicated for each user. Each codebook consists of four different complex codewords representing four different information symbols $\{0, 1, 2, 3\}$. Depending on the input data, one codeword is selected by each user denoted by $\{x_1, x_2, \dots, x_6\}$ for transmission where, $x_j \in \mathbb{C}^{4 \times 1}$, $j = 1, \dots, 6$. The performance of an SCMA system is highly sensitive to the codebooks.

2) *Factor Graph*: Observe from Fig. 2 that the codewords of any particular codebook are sparse and contain 0s in specific locations. For any user, if a codeword has a non-zero element in the j^{th} location, then it implies that the user is occupying the j^{th} resource. The sharing of resources amongst multiple users can be graphically represented by a factor graph. The factor graph for a $J \times K$ SCMA system contains J user nodes

and K resource/factor nodes. An edge is assigned between the j^{th} user node and the k^{th} resource node only if the j^{th} user occupies the k^{th} resource. Fig. 3 shows the factor graph for the SCMA model described in Fig. 2. The degrees of a user node and a resource/factor node are denoted by d_u and d_f respectively. For the factor graph shown in Fig. 3, we have $d_u = 2$ and $d_f = 3$. An alternative of the factor graph is the

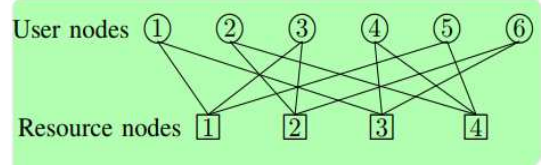


Fig. 3: Factor graph for $J = 6$, $K = 4$ SCMA system.

factor matrix, \mathbf{F} . Each edge in the factor graph is denoted by a '1' in the factor matrix. For the factor graph shown in Fig. 3, \mathbf{F} is obtained as given below:

$$\mathbf{F} = \begin{bmatrix} 1 & 0 & 1 & 0 & 1 & 0 \\ 0 & 1 & 1 & 0 & 0 & 1 \\ 1 & 0 & 0 & 1 & 0 & 1 \\ 0 & 1 & 0 & 1 & 1 & 0 \end{bmatrix}. \quad (12)$$

The sparsity of factor graph or matrix indicates that MPA can be used in SCMA detection. It is extensively reported in literature that the MPA-based detection provides excellent performance in SCMA [7, 19].

3) *Downlink*: In downlink, the base station (BS) first sums up the codewords of all J users. This superimposed signal is broadcast to every user. The received signal $\mathbf{y}_i = [y_{i1}, \dots, y_{iK}]^T$ at the i^{th} user can be expressed as

$$\mathbf{y}_i = \text{diag}(\mathbf{h}_i) \sum_{j=1}^J \mathbf{x}_j + \mathbf{n}_i \quad (13)$$

where, $\mathbf{h}_i = [h_{i1}, h_{i2}, \dots, h_{iK}]$ is the channel impulse response vector between the BS and the i^{th} user, \mathbf{n}_i is the AWGN at the i^{th} user and is complex Gaussian distributed, i.e., $\mathbf{n}_i \sim \mathcal{CN}(0, N_0 \mathbf{I}_K)$.

4) *Uplink*: In uplink, each user incorporates the respective channel to transmit the information to the BS. The BS receives the signal \mathbf{y} which is given by

$$\mathbf{y} = \sum_{j=1}^J \text{diag}(\mathbf{h}_j) \mathbf{x}_j + \mathbf{n} \quad (14)$$

where, \mathbf{n} is the AWGN at the BS.

III. PROPOSED METHOD OF SCMA-BASED OTFS-NOMA

In this section we propose the system model for OTFS-SCMA for downlink and uplink. The operations to be carried out in the transmitter and the receiver side are described in details in the following.

A. In Downlink

Consider a downlink scenario with J receiving users and one transmitting BS as shown in Fig. 4. Note that only the

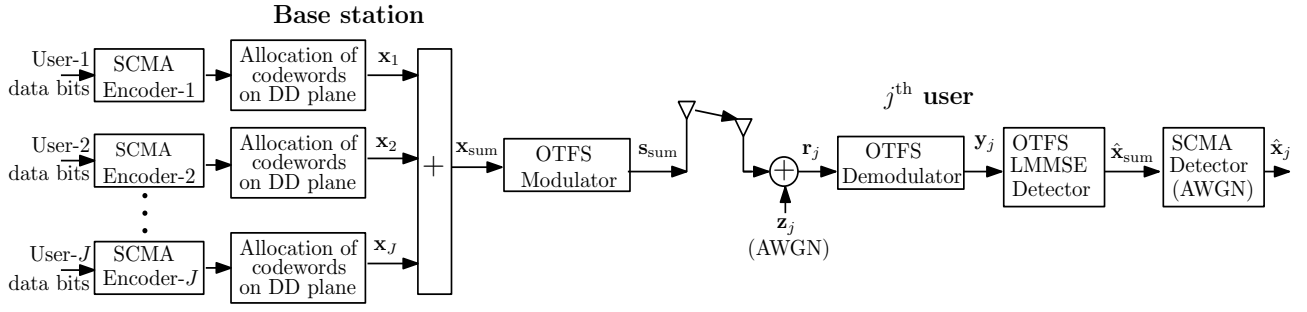


Fig. 4: Block diagram of OTFS-SCMA in downlink.

j^{th} user's receiver is depicted. A $J \times K$ SCMA system is considered with overloading factor $\lambda = \frac{J}{K}$. The length of a complex SCMA codeword is K . For allocation of the SCMA codewords over the delay-Doppler plane, we consider two schemes:

Scheme 1: The SCMA codewords for the j^{th} user, $j = 1, \dots, J$ are allocated in the delay-Doppler plane $\Gamma_{M,N}$ along the Doppler direction in blocks of size $K \times 1$. This scheme is depicted in Fig. 5 for $M = 8, N = 8$ and $K = 4$.

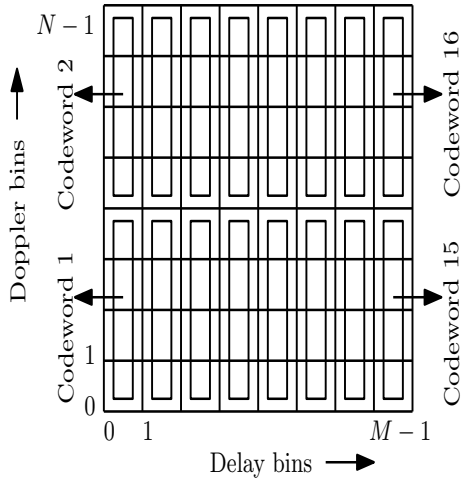


Fig. 5: Allocation of SCMA codewords of length $K = 4$ in delay-Doppler plane $\Gamma_{8,8}$, *Scheme 1*.

Scheme 2: The SCMA codewords for the j^{th} user, $j = 1, \dots, J$ are allocated in the delay-Doppler plane $\Gamma_{M,N}$ along the delay direction in blocks of size $1 \times K$. This scheme is depicted in Fig. 6 for $M = 8, N = 8$ and $K = 4$.

The $J \times K$ SCMA system is referred to as the *basic SCMA system* as it is repeated over the delay-Doppler grid multiple times. In the following, we present the method for Scheme 1. The notations and the methods can be easily extended to Scheme 2.

There are $M \times N$ slots for complex numbers in $\Gamma_{M,N}$. Thus, for every user, the total number of symbols that can be accommodated inside $\Gamma_{M,N}$ is $N_{\text{sym}} = \frac{M \times N}{K}$ as the length of any SCMA codeword is K . Suppose $\mathbf{x}_j \in \mathbb{C}^{N \times M}$ is the input delay-Doppler frame for j^{th} user. The superimposed

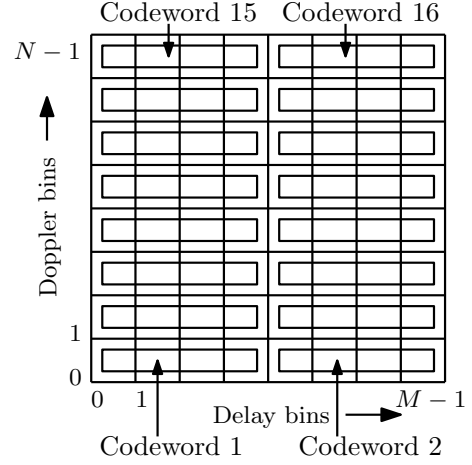


Fig. 6: Allocation of SCMA codewords of length $K = 4$ in delay-Doppler plane $\Gamma_{8,8}$, *Scheme 2*.

input signal is given by

$$\mathbf{x}_{\text{sum}} = \sum_{j=1}^J \mathbf{x}_j \quad (15)$$

where, the summation is done bin-wise. The superposition of the SCMA codewords of all users is depicted in Fig. 7 for $\Gamma_{4,4}$ and 6×4 SCMA system. Note that the delay-Doppler plane of each user contains a significant number of 0s as the SCMA codewords are sparse. The superimposed signal \mathbf{x}_{sum}

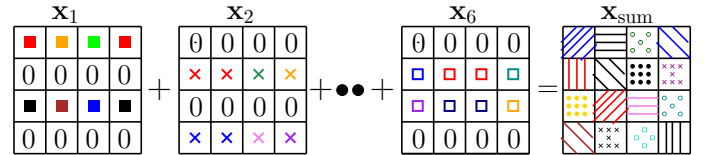


Fig. 7: Superposition of SCMA codewords of all users in delay-Doppler plane $\Gamma_{4,4}$ with 6×4 SCMA system.

goes through the OTFS modulator to produce the vector $\mathbf{s}_{\text{sum}} \in \mathbb{C}^{MN \times 1}$. The BS transmits \mathbf{s}_{sum} and signal \mathbf{r}_j received by the j^{th} user is passed through an OTFS demodulator. Suppose the output of the OTFS demodulator is \mathbf{y}_j .

Invoking the input-output relationship between the BS and the j^{th} user, \mathbf{y}_j can be written in terms of the superposition \mathbf{x}_{sum} of the input SCMA codewords. Suppose $\mathbf{x}_{\text{sum,vec}} \in$

$\mathbb{C}^{MN \times 1}$ and $\mathbf{y}_{j,\text{vec}} \in \mathbb{C}^{MN \times 1}$ are the row-wise vectorized versions of $\mathbf{x}_{\text{sum}} \in \mathbb{C}^{N \times M}$ and $\mathbf{y}_j \in \mathbb{C}^{N \times M}$ respectively. The effective input-output relation now becomes

$$\mathbf{y}_{j,\text{vec}} = \mathbf{H}_j \mathbf{x}_{\text{sum,vec}} + \mathbf{z}_j \quad (16)$$

where, \mathbf{H}_j is the $NM \times NM$ complex coefficient matrix specifying the relationship between the input $\mathbf{x}_{\text{sum,vec}}$ and output $\mathbf{y}_{j,\text{vec}}$, and $\mathbf{z}_j \in \mathbb{C}^{MN \times 1}$ is the complex AWGN.

As the BS is transmitting $J \times N_{\text{sym}}$ symbols over $M \times N$ resources, the overloading factor of the OTFS-SCMA scheme becomes $\lambda = \frac{J \times N_{\text{sym}}}{M \times N} = \frac{J}{K}$. Thus the overloading factor of the OTFS-SCMA system is exactly equal to the underlying basic SCMA system.

Observe from (16) that in order to recover $\mathbf{x}_{\text{sum,vec}}$ from $\mathbf{y}_{j,\text{vec}}$, any OTFS detector can be used. We propose to use a simple LMMSE-based detector for the same. The estimate of $\mathbf{x}_{\text{sum,vec}}$ is obtained as

$$\hat{\mathbf{x}}_{\text{sum,vec}} = \mathbf{H}_j^* [\mathbf{H}_j \mathbf{H}_j^* + \sigma_n^2 \mathbf{I}_{MN}]^{-1} \mathbf{y}_{j,\text{vec}}. \quad (17)$$

Note that (17) involves matrix inversion which increases the computational complexity. In order to lower the complexity, the method proposed in [17] may be used for OTFS detection. The output $\hat{\mathbf{x}}_{\text{sum,vec}}$ of the LMMSE detector is fed to an MPA-based SCMA detector block to obtain the estimate $\hat{\mathbf{x}}_j$ of the j^{th} user's data \mathbf{x}_j . Note that the SCMA-detection block contains N_{sym} basic SCMA detectors. Moreover, as the effects of fading have been canceled by the OTFS detector, we consider a simple AWGN channel for the SCMA detector.

B. In Uplink

Consider an uplink scenario with J transmitting users and one receiving BS as shown in Fig. 8. The description of the methods pertains to Scheme 1. The SCMA codewords are allocated as depicted in Fig. 5. There are J input-output relations between the output of the OTFS demodulator \mathbf{y} and inputs \mathbf{x}_j of each user's modulator, $j = 1, \dots, J$. Combining these J relations, the vectorized version \mathbf{y}_{vec} of \mathbf{y} can be expressed as

$$\mathbf{y}_{\text{vec}} = \sum_{j=1}^J \mathbf{H}_j \mathbf{x}_{j,\text{vec}} + \mathbf{z} \quad (18)$$

where, $\mathbf{z} \in \mathbb{C}^{MN \times 1}$ is the complex AWGN.

Unlike in downlink, the receiver in uplink involves more than one \mathbf{H} matrices. Therefore, the previously-discussed two-stage method of detection cannot be adopted here. From (18), \mathbf{y}_{vec} can be written as

$$\mathbf{y}_{\text{vec}} = \mathbf{H}_{\text{all}} \mathbf{x}_{\text{all}} + \mathbf{z} \quad (19)$$

where,

$$\mathbf{H}_{\text{all}} = [\mathbf{H}_1, \mathbf{H}_2, \dots, \mathbf{H}_J] \quad \text{and} \quad (20)$$

$$\mathbf{x}_{\text{all}} = [\mathbf{x}_{1,\text{vec}}, \mathbf{x}_{2,\text{vec}}, \dots, \mathbf{x}_{J,\text{vec}}]^T$$

Observe from (20) that \mathbf{H}_{all} is an $MN \times JMN$ complex matrix and \mathbf{x}_{all} is the information vector of length JMN . However, as \mathbf{x}_{all} contains SCMA codewords, it will be a sparse vector. The number of 0s in \mathbf{x}_{all} is $\frac{JMN d_v}{K}$, where d_v is the

number of non-zero components in a length- K codeword of an $J \times K$ SCMA system. For an SCMA system with factor graph shown in Fig. 3, \mathbf{x}_{all} contains $3MN$ non-zero complex numbers. Let $\mathbf{x}_{\text{all,compr}}$ denote the compressed input vector after removing the 0s in \mathbf{x}_{all} . Similarly, let $\mathbf{H}_{\text{all,compr}}$ denote the effective compressed \mathbf{H} matrix after deleting the columns corresponding to the locations of the 0s in \mathbf{x}_{all} . Then, the input-output relationship in (19) can now be written as

$$\mathbf{y}_{\text{vec}} = \mathbf{H}_{\text{all,compr}} \mathbf{x}_{\text{all,compr}} + \mathbf{z} \quad (21)$$

where, $\mathbf{H}_{\text{all,compr}} \in \mathbb{C}^{MN \times \frac{JMN d_v}{K}}$ and $\mathbf{x}_{\text{all,compr}} \in \mathbb{C}^{\frac{JMN d_v}{K} \times 1}$.

Observe from (21), that we have less observations than the number of variables. Therefore, a powerful detector must be employed in the receiver. We consider a single stage of MPA for the detection. Note that the consecutive d_v elements of $\mathbf{x}_{\text{all,compr}}$ are the non-zero elements of a particular SCMA codeword. These d_v elements should be considered together as a single entity or observation node as they correspond to a particular information symbol in the input side.

In (21), we consider $\mathbf{x}_{\text{all,compr}} \in \mathbb{C}^{\frac{JMN d_v}{K} \times 1}$ as a collection of $\frac{JMN}{K}$ variable nodes. We call them variable nodes (not user nodes) as they refer to different symbols of the same user. Each variable node comprises of d_v complex numbers but they all refer to one particular symbol. Similarly, in every row of $\mathbf{H}_{\text{all,compr}}$, the consecutive d_v complex coefficients must be clubbed together. With these new conventions, (21) can be written as

$$\mathbf{y}_{\text{vec}} = \begin{bmatrix} y_1 \\ \vdots \\ y_{MN} \end{bmatrix} = \begin{bmatrix} \mathbf{h}_{1,1} & \cdots & \mathbf{h}_{1,\frac{JMN}{K}} \\ \vdots & \ddots & \vdots \\ \mathbf{h}_{MN,1} & \cdots & \mathbf{h}_{MN,\frac{JMN}{K}} \end{bmatrix} \begin{bmatrix} \mathbf{x}_1 \\ \vdots \\ \mathbf{x}_{\frac{JMN}{K}} \end{bmatrix} + \begin{bmatrix} z_1 \\ \vdots \\ z_{MN} \end{bmatrix}. \quad (22)$$

In (22), for any d and c , $\mathbf{h}_{dc} \in \mathbb{C}^{1 \times d_v}$ and $\mathbf{x}_c \in \mathbb{C}^{d_v \times 1}$. The corresponding factor graph comprises of MN observation nodes and $\frac{JMN}{K}$ variable nodes. An edge is assigned between the observation node y_d and the variable node \mathbf{x}_c if $\mathbf{h}_{dc} \neq [0, \dots, 0]_{1 \times d_v}$. The set of variable nodes connected to the d^{th} observation node is denoted by \mathcal{M}_d and $\mathcal{M}_d^c = \mathcal{M}_d \setminus \{c\}$. Similarly, \mathcal{N}_c denotes the set of observation nodes connected to the c^{th} variable node and $\mathcal{N}_c^d = \mathcal{N}_c \setminus \{d\}$. The MPA-based detection is carried out over this factor graph. Algorithm 1 presents the detailed procedures of the detection process. In MPA, the message update from an observation node is very critical and this step is further explained with the help one example furnished below.

Example 1. Consider a $J = 6$ and $K = 4$ SCMA system as shown in Fig. 3 and a delay-Doppler plane with $M = 4$ and $N = 4$. Each user allocates 4 SCMA codewords over one frame. The numbers of observation nodes and variable nodes are 16 and 24 respectively. Suppose the observation node y_d is connected to the variable nodes $\{c, c_1, c_2\}$ through the coefficient vectors $\{\mathbf{h}_{dc}, \mathbf{h}_{dc_1}, \mathbf{h}_{dc_2}\}$ respectively. The situation is shown in Fig. 9. Here the lengths of each coefficient vector and symbol vector are equal to $d_v = 2$.

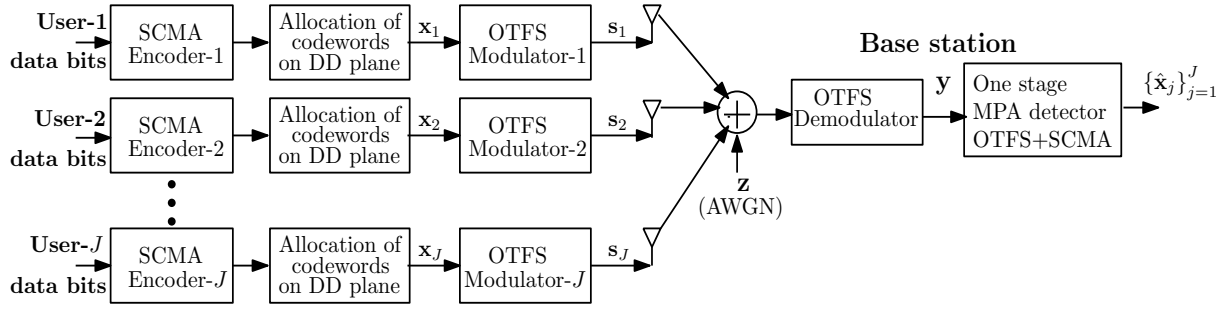


Fig. 8: Block diagram of OTFS-SCMA in uplink.

Algorithm 1: MPA-based detection for OTFS-SCMA in uplink

input : \mathbf{y}_{vec} , $\mathbf{H}_{\text{all,compr}}$, Alphabets $\{\mathbb{A}_j\}_{j=1}^J$, $\frac{E_b}{N_0}$
output: Estimated data symbol for $\hat{\mathbf{x}}_{\text{all,compr}}$

Initialization: For every $c \in \{1, \dots, JMN/K\}$ and for every $d \in \mathcal{N}_c$, set $V_{c \rightarrow d}^{(0)}(\mathbf{x}_{cm}) = 1/A$, $m = 1, \dots, A$, where A is the size of the alphabet, Iteration index $l \leftarrow 0$;
while termination criteria not fulfilled **do**
 for $d \leftarrow 1$ **to** MN **do**
 foreach $c \in \mathcal{M}_d$ **do**
 Compute $U_{d \rightarrow c}^{(l)}(\mathbf{x}_{cm})$ for $m = 1, \dots, A$

$$U_{d \rightarrow c}^{(l)}(m) = \sum_{\mathbf{v} \in \mathcal{V}_{dc}} \frac{1}{\pi N_0} \exp[-\frac{1}{N_0} |y_d - \mathbf{h}_{dc} \mathbf{x}_{cm} - \sum_{c' \in \mathcal{M}_d^c} \mathbf{h}_{dc'} \mathbf{v}_{c'}|^2] \prod_{c' \in \mathcal{M}_d^c} V_{c' \rightarrow d}^{(l-1)}(\mathbf{v}_{c'})$$

 where, $\mathcal{V}_{dc} = \prod_{c' \in \mathcal{M}_d^c} \mathbb{A}_{c'}$ is the Cartesian product of alphabets with $\mathbf{v} = [\mathbf{v}_{c'}]_{c' \in \mathcal{M}_d^c}$ is a member of \mathcal{V}_{dc} and $\mathbf{v}_{c'} \in \mathbb{A}_{c'}$
 Normalization $U_{d \rightarrow c}^{(l)}(\mathbf{x}_{cm}) = \frac{U_{d \rightarrow c}^{(l)}(\mathbf{x}_{cm})}{\sum_{m'=1}^A U_{d \rightarrow c}^{(l)}(\mathbf{x}_{cm'})}$
 for $c \leftarrow 1$ **to** JMN/K **do**
 foreach $d \in \mathcal{N}_c$ **do**
 Compute $V_{c \rightarrow d}^{(l)}(\mathbf{x}_{cm})$ for $m = 1, \dots, A$

$$V_{c \rightarrow d}^{(l)}(\mathbf{x}_{cm}) = \prod_{d' \in \mathcal{N}_c^d} U_{d' \rightarrow c}^{(l)}(\mathbf{x}_{cm})$$

 Normalization $V_{c \rightarrow d}^{(l)}(\mathbf{x}_{cm}) = \frac{V_{c \rightarrow d}^{(l)}(\mathbf{x}_{cm})}{\sum_{m'=1}^A V_{c \rightarrow d}^{(l)}(\mathbf{x}_{cm'})}$
 for $c \leftarrow 1$ **to** JMN/K **do**
 Compute $V_c^{(l)}(\mathbf{x}_{cm})$ for $m = 1, \dots, A$

$$V_c(\mathbf{x}_{cm}) = \prod_{k \in \mathcal{N}_c} U_{d \rightarrow c}^{(l)}(\mathbf{x}_{cm}).$$

 If the posterior probability values \mathbf{V}_c converge or the maximum number of iterations is exhausted, then stop and proceed for decision making in following step .
 Otherwise, set $l = l + 1$ and continue.
 Decision: $\hat{\mathbf{x}}_c = \arg \max_{\mathbf{x}_{cm} \in \mathbb{A}_c} V_c(\mathbf{x}_{cm})$, $c = 1, \dots, JMN/K$

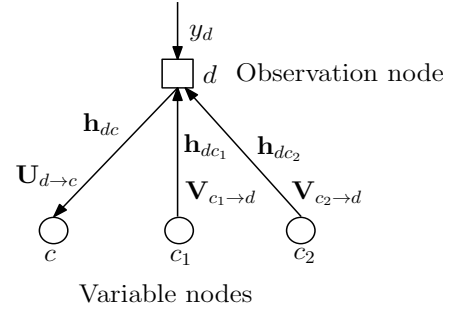


Fig. 9: Observation node update in the single-stage MPA detection of OTFS-SCMA in uplink.

The message $U_{d \rightarrow c}$ from the observation node d to the user node c is given by

$$U_{d \rightarrow c}^{(l)}(m) = \sum_{(\mathbf{v}_{c_1}, \mathbf{v}_{c_2}) \in \mathbb{A}_{c_1} \times \mathbb{A}_{c_2}} \frac{1}{\pi N_0} \exp[-\frac{1}{N_0} |y_d - \mathbf{h}_{dc} \mathbf{x}_{cm} - \mathbf{h}_{dc_1} \mathbf{v}_{c_1} - \mathbf{h}_{dc_2} \mathbf{v}_{c_2}|^2] V_{c_1 \rightarrow d}^{(l-1)}(\mathbf{v}_{c_1}) V_{c_2 \rightarrow d}^{(l-1)}(\mathbf{v}_{c_2}) \quad (23)$$

Suppose, the size of each alphabet is $A = 4$. Each alphabet contains 4 codewords of length $d_v = 2$. The Cartesian product $\mathbb{A}_{c_1} \times \mathbb{A}_{c_2}$ contains $4^2 = 16$ combinations of $(\mathbf{v}_{c_1}, \mathbf{v}_{c_2})$ and the outer summation in (23) is done over these 16 combinations. Observe that the product $\mathbf{h}_{dc_i} \mathbf{v}_{c_i}$ is a scalar complex number and thus the argument in the exponential term in (23) is scalar.

The computation of the messages from the variable nodes are relatively simple. The outgoing message from a variable node to an observation node is given by the component-wise product of the incoming messages from the other connected observation nodes. The *a posteriori* probability values of the variable nodes are computed by component-wise multiplication of all incoming messages from the neighboring observation nodes. The estimate of a variable node is considered as that symbol in the alphabet for which the *a posteriori* probability value becomes the maximum. The details are given in Algorithm 1.

We present a theorem without proof regarding the degrees of the observation and the variable nodes in the effective factor graph in uplink. This theorem is crucial for the complexity analysis of detection process.

Theorem 1. Consider an OTFS-SCMA model with $J \times K$ SCMA system in uplink. Let the degrees of a variable node and a resource node in the basic SCMA system are d_v and d_f respectively. Let P denote the number of multipaths for the underlying wireless channels for each user. Suppose for every user, the values l_{τ_i}, k_{ν_i} , $i = 1, \dots, P$ are generated randomly from $\{0, \dots, P-1\}$. Then for the effective factor graph of the OTFS-SCMA system free of fractional Doppler, the degrees $\{d_{v_i}^{\text{eff}}\}_{i=1}^{\frac{JMN}{K}}$ of the variable nodes and the degrees $\{d_{f_i}^{\text{eff}}\}_{i=1}^{MN}$ of the observation nodes satisfy the following:

$$\begin{aligned} \frac{1}{\left(\frac{JMN}{K}\right)} \sum_{i=1}^{\frac{JMN}{K}} d_{v_i}^{\text{eff}} &\leq P d_v \\ \frac{1}{MN} \sum_{i=1}^{MN} d_{f_i}^{\text{eff}} &\leq P d_f \end{aligned} \quad (24)$$

Complexity Analysis

Here, the complexity of the proposed method is analyzed for downlink and uplink. As the complexity is mainly contributed by the sophisticated detectors in the receiver side, we focus on the complexity of the detectors only.

Downlink: The detector in downlink is a concatenated system of LMMSE detector and MPA detector. The interference over the delay-Doppler plane is removed by the LMMSE-based OTFS detector. The LMMSE detector involves traditional matrix inversion. Its complexity is $O(M^3 N^3)$. If the low-complexity version of LMMSE detector in [17] is used, then the complexity would be $O\left(\frac{MN}{2} \log_2 N + 2MN P^2\right)$. The output of the OTFS detector now contains the multi-user interference. The MPA-based SCMA detector removes multi-user interference. The complexity of the SCMA detector is $O\left(\frac{MN}{K} A^{d_f}\right)$ where, A is the alphabet size. For relatively small values of M and N , the complexity of the two-stage detector is approximately $O(A^{d_f})$.

Uplink: In uplink, the detector comprises of only a single MPA. As per Theorem 1, the average degree of an observation node in the effective factor graph is upper bounded by $P d_f$, where d_f is the degree of the factor node in the basic SCMA system and P is the number of multipaths. Therefore, the complexity of the detector in uplink is $O(MN A^{P d_f})$ as there are MN observation nodes. Note that the complexity of this detector is high if the number of multipaths is high. If P is known to be high in a particular situation, then in place of the MPA described in Algorithm 1, other variants based on expectation propagation [20], Gaussian-approximated MPA [14] etc. may be used to reduce the complexity.

Remark 1. Here we further clarify the use of two-stage and single-stage detectors in downlink and uplink respectively. Observe from (16) that in downlink, the delay-Doppler and multi-user interactions are separable. The matrix \mathbf{H}_j corresponds to the delay-Doppler interaction and the superimposed signal $\mathbf{x}_{\text{sum,vec}}$ arises due to multi-user fusion. On the other hand, observe from (18) that the delay-Doppler and multi-

user interactions are not separable in uplink. Therefore, the combined approach of OTFS and SCMA detection must be adopted. Note that this combined or single stage of detection can also be considered in downlink. However, due to high complexity of the combined detector, two stage approach is followed in downlink.

IV. SIMULATION RESULTS

In this section, we present the bit-error rate (BER) simulation results for uncoded OTFS-SCMA systems. The results for both downlink and uplink are presented. In both cases, we consider OTFS with rectangular pulse. The OTFS system is assumed to free of fractional Doppler and fractional delay values. It is assumed that the receiver has the perfect knowledge of the channel. We also compare the results of the proposed NOMA system with those of conventional OMA schemes over QAM alphabets. In order to compute the BER at any SNR, Monte Carlo simulation is carried out for 5×10^4 frames.

A. Downlink

First we consider a delay-Doppler plane $\Gamma_{8,8}$. An SCMA system with $J = 6$ and $K = 4$ is considered. The SCMA codebooks proposed in [21] are used. The overloading factor of the OTFS-SCMA system is $\lambda = J/K = 150\%$. The BS transmits $MN/K = 16$ symbols for each user. First, as per Scheme 1, 16 SCMA codewords of every user are allocated on respective delay-Doppler plane. The BS then superimposes the input signals over these 6 delay-Doppler grids. The superimposed signal is fed to the OTFS modulator which comprises of ISFFT and Heisenberg transforms. The modulator output is transmitted over the wireless channel.

The wireless channel is represented by P propagation paths. The i^{th} path is associated with integer delay (l_{τ_i}) and Doppler (k_{ν_i}) components as explained in Section II-A3. We consider $\Delta f = 1$ and $T = 1$. One of P paths is the line-of-sight (LoS) path with ($l_{\tau_i} = 0, k_{\nu_i} = 0$). The remaining values of l_{τ_i} s and k_{ν_i} s are generated randomly from $\{0, \dots, P-1\}$. In our simulations, we have considered distinct propagation paths with distinct pairs of (l_{τ_i}, k_{ν_i}).

The received signal is passed through the OTFS demodulator, OTFS LMMSE detector and SCMA detector block sequentially as shown in Fig. 4. The BER performance of this OTFS-NOMA scheme is presented in Fig. 10. The results for $P = 2, 3, 4$ are shown. Observe that as P increases, the BER curve improves. This improvement may be attributed to the increased diversity in the system [22, 23].

Fig. 10 also presents results for OTFS-OMA over $\Gamma_{8,8}$. The OTFS-OMA scheme proposed in [10] is considered first. We consider two users occupying the delay-Doppler plane as shown in Fig. 11. Each user's QAM symbols are placed in the plane in a non-overlapping manner as depicted in Fig. 11. Observe that the number of symbols that can be transmitted by each user is 32. Thus for two users, the BS transmits 64 symbols over 64 slots in the plane. The overloading factor is 100%. LMMSE-based detector is used

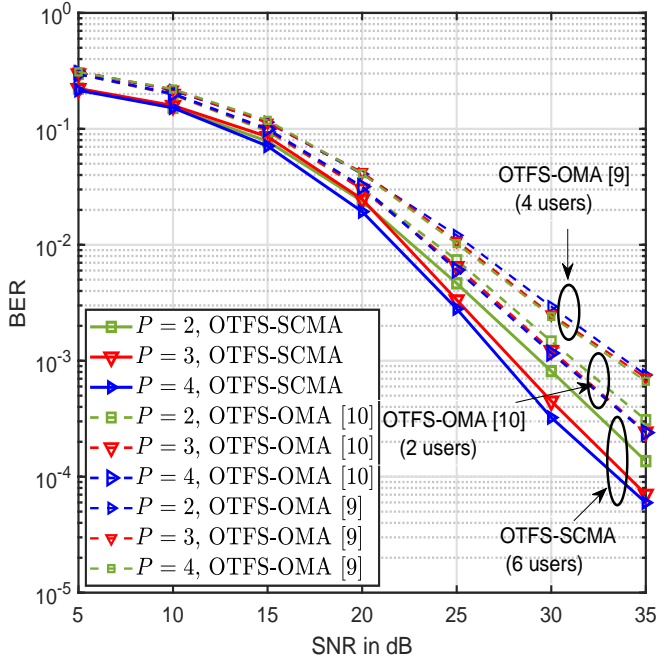


Fig. 10: OTFS-SCMA with $N = 8$, $M = 8$ and ($J = 6$, $K = 4$) SCMA system, overloading factor 150%, (Scheme 1) in downlink.

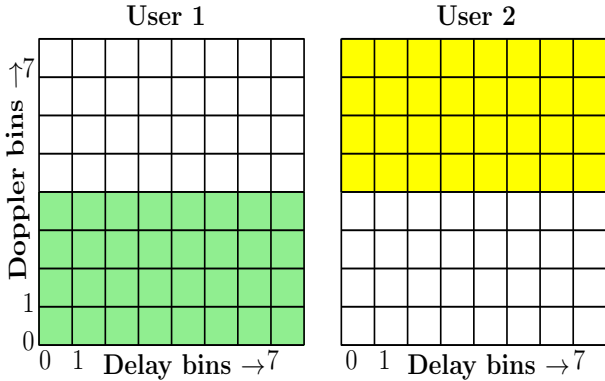


Fig. 11: OTFS-OMA with $N = 8$, $M = 8$ with two users [10] in downlink.

after OTFS demodulator. We have also considered the OTFS-OMA method proposed in [9] for 4 users. The symbols of the 4 users are placed on $\Gamma_{8,8}$ as shown in Fig. 12. Here also, the overloading factor is 100%.

The BER results for these OMA schemes with $P = 2, 3, 4$ are shown in Fig. 10. We consider QAM alphabet as its size ($A = 4$) is exactly same as that of the OTFS-SCMA system under consideration. Observe that, even though the OTFS-SCMA system involves 6 users with overloading factor 150%, it performs better than the OTFS-OMA schemes with 2 users and 4 users with overloading factor of 100%. Remark 2 explains the performance improvement of OTFS-SCMA over OTFS-OMA.

Next, we consider an SCMA system with $J = 8$ and $K = 4$. The overloading factor of this OTFS-SCMA scheme is 200%.

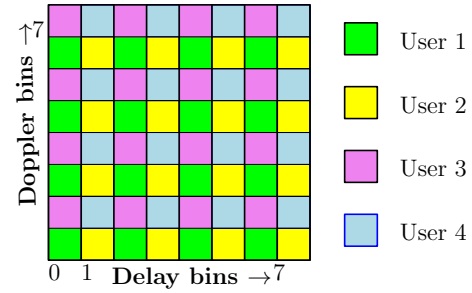


Fig. 12: OTFS-OMA with $N = 8$, $M = 8$ with four users [9] in downlink.

The 4×6 factor matrix \mathbf{F} shown in (12) is enlarged to the following 4×8 factor matrix \mathbf{F}_e :

$$\mathbf{F}_e = \begin{bmatrix} 1 & 0 & 1 & 0 & 1 & 0 & 1 & 0 \\ 0 & 1 & 1 & 0 & 0 & 1 & 1 & 0 \\ 1 & 0 & 0 & 1 & 0 & 1 & 0 & 1 \\ 0 & 1 & 0 & 1 & 1 & 0 & 0 & 1 \end{bmatrix} \quad (25)$$

Note from (25) that \mathbf{F}_e is obtained from \mathbf{F} by appending the 3rd and the 4th columns of \mathbf{F} to itself sequentially. In \mathbf{F}_e , the 7th and 8th columns are identical to the 3rd and the 4th respectively. Observe from (25) that the 3rd and the 4th columns are non-overlapping. Therefore, the codebooks for the 7th and the 8th users are set exactly to those for the 4th and the 3rd users respectively. These codebooks are used for the OTFS-SCMA modulation. Fig. 13 presents the BER performance of the

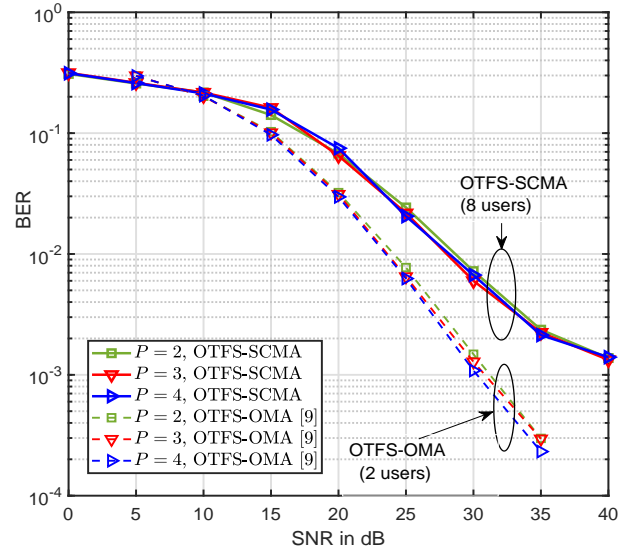


Fig. 13: OTFS-SCMA with $N = 8$, $M = 8$ and ($J = 8$, $K = 4$) SCMA system, overloading factor 200% in downlink.

OTFS-SCMA system with Scheme 1 in downlink. Although the overloading factor is 200%, the BER performance is impressive. This performance is compared with OTFS-OMA method [9] for 2 users. Note that the performance of the OTFS-SCMA with an overloading factor of 200% is worse than OTFS-OMA with 2 users. The plots in Fig. 13 shows that the BER performance is almost similar for $P = 2, 3, 4$.

This observation may arise due to excessive overloading and repetition of a few codebooks amongst users.

Now we consider a delay-Doppler plane $\Gamma_{M,N}$ with unequal values of M and N and compare the performances of Scheme 1 and Scheme 2 which are described in Section IV-A. We consider $M = 16$ and $N = 8$. A 6×4 SCMA system is adopted. Fig. 14 presents the BER performances of the schemes for $P = 2$ and $P = 4$. For $P = 2$, Scheme 1 performs slightly better than Scheme 2. However, as P increases, it has been observed that the performances of both Scheme 1 and Scheme 2 are similar.

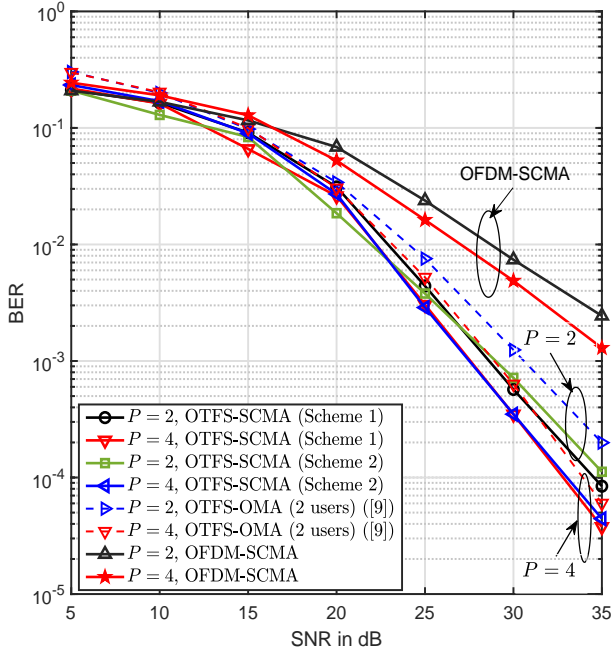


Fig. 14: OTFS-SCMA with $N = 8$, $M = 16$ and ($J = 6$, $K = 4$) SCMA system (Scheme 1 and Scheme 2) in downlink.

Fig. 14 also shows the performance of the OFDM-SCMA system. The same simulation set-up of OTFS-SCMA is considered here. The delay-Doppler channel representation is used. The only difference is that the information symbols are directly put on the time-frequency domain. In other words, the ISFFT and the SFFT transformations are not considered in the modulator and the demodulator respectively. Observe that the performance of OFDM-SCMA is not satisfactory. There is a significant performance gain of OTFS-SCMA over OFDM-SCMA. This observation in the multi-user scenario is in agreement with the result reported in [14] for the single-user case.

B. Uplink

Here we present the simulation results for OTFS-SCMA with different values of M and N in uplink. First we consider delay-Doppler plane with $M = 4$, $N = 4$ and $J = 6$, $K = 4$ SCMA system. In this section, Scheme 1 is used for allocating the SCMA codewords over the delay-Doppler plane. Each

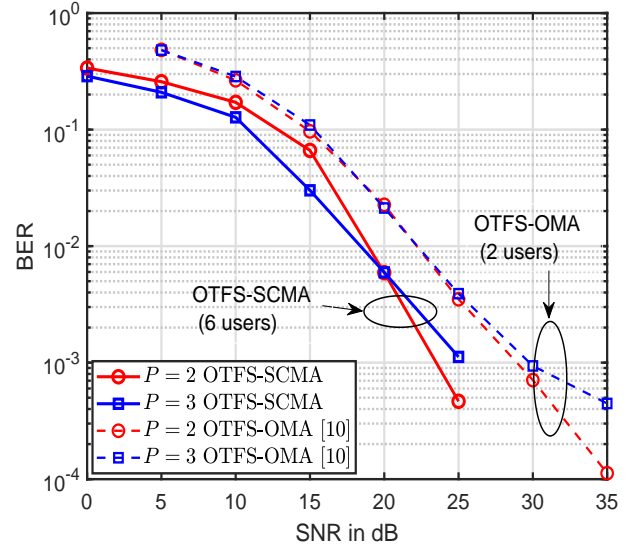


Fig. 15: OTFS-SCMA with $N = 4$, $M = 4$ and ($J = 6$, $K = 4$) SCMA system and OTFS-OMA over QAM in uplink.

of the 6 users places 4 SCMA codewords over the delay-Doppler plane $\Gamma_{4,4}$. Thus the overloading factor becomes $\lambda = 24/16 = 150\%$. The respective output of the OTFS modulator is transmitted over the channel towards the BS. The BS receiver first feed the signal from the channel to an OTFS demodulator. The effective coefficient matrix \mathbf{H} is found out as explained in Section III-B. Then using this matrix, the single-stage MPA-based detection is carried out to extract the individual users' data symbols. Note that this detector acts as the combined detector of OTFS and SCMA symbols. Fig. 15 shows the BER plots for the proposed OTFS-SCMA scheme for $P = 2$ and $P = 3$. The results of OTFS-OMA [10] with 2 users are also shown in Fig. 15. 4-QAM is considered for OTFS-OMA. The QAM symbols are placed in the delay-Doppler grid $\Gamma_{4,4}$ in the same way as depicted in Fig. 11. For OTFS-OMA in uplink, the detection is carried out with the help of MPA. Note that in uplink too, the OTFS-SCMA performs significantly better than its OMA counterpart. Moreover, the performance of the proposed OTFS-SCMA is better in uplink than in downlink. This performance difference may be accredited to the combined powerful MPA detector in uplink compared to the two stage detection process in downlink. Note that the BER for $P = 3$ tends to be worse than that for $P = 2$ after a certain SNR value for both OTFS-SCMA and OTFS-OMA. This peculiar transition happens as the value of $P = 3$ is close to the number of delay (M) and Doppler (N) bins.

Next we consider a delay-Doppler grid $\Gamma_{4,8}$ with $J = 6$, $K = 4$ SCMA system. Fig. 16 presents the BER plots for the proposed OTFS-SCMA system for $P = 2$ and $P = 4$. Observe that as P increases the BER improves due to the enhancement of the diversity. The results of OTFS-OMA [9, 10] are also shown in Fig. 16. Here also, the OTFS-SCMA performs better than OTFS-OMA over the alphabets of same size.

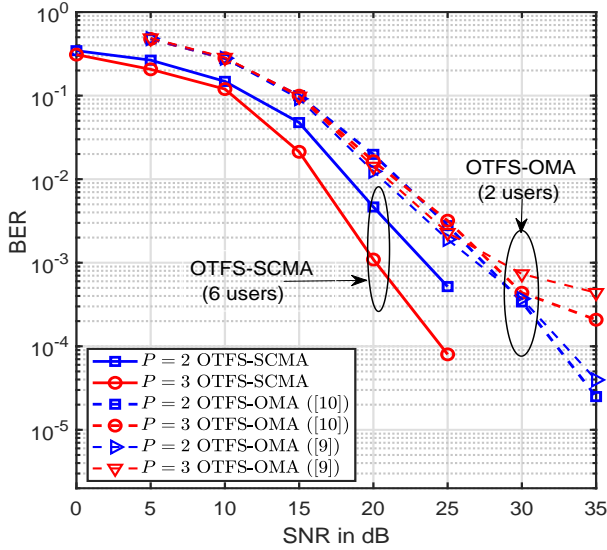


Fig. 16: OTFS-SCMA with $N = 4$, $M = 8$ and ($J = 6$, $K = 4$) SCMA system and OTFS-OMA over QAM in uplink.

Remark 2. Observe from Fig. 10, Fig. 14, Fig. 15 and Fig. 16 that the proposed OTFS-SCMA method outperforms the conventional OTFS-OMA schemes [9, 10] in both downlink and uplink. Note that the alphabets of OTFS-SCMA system contain codeword vectors of length $K = 4$ for a 6×4 SCMA system. The detection is done vector-wise. Moreover, SCMA codebooks can offer impressive coding and shaping gain [7]. On the other hand, in OTFS-OMA, the alphabet is the standard 4-QAM where any codeword is a scalar complex. These facts contribute towards the performance gain of OTFS-SCMA over OTFS-OMA.

V. CONCLUSIONS

This paper presented a novel OTFS-NOMA strategy based on SCMA. This proposed method considers pre-designed SCMA codebooks with a particular overloading factor. The sparse SCMA codewords of each user are placed on the delay-Doppler grid either vertically or horizontally. The ratio of the total number of codewords or symbols transmitted by all users to the total number slots or resources in the delay-Doppler plane is exactly equal to the overloading factor of the underlying basic SCMA system. The proposed OTFS-SCMA scheme has been devised and analyzed for both downlink and uplink. The receiver in downlink includes a two stage detection process. First, the intermingling of the symbols in different delay-Doppler slots is resolved with the help of an OTFS detector. Subsequently, an SCMA detector eliminates the multi-user interaction. In uplink, the receiver in the BS comprises of a combined OTFS-SCMA detector based on a single-stage of MPA. Both delay-Doppler and multi-user interactions are resolved at one shot. Simulation results are presented with different parameters for both the cases of downlink and uplink with overloading factor upto 200%. The results showed that the proposed OTFS-SCMA system can

yield better BER performances than the conventional OTFS-OMA systems.

REFERENCES

- [1] Ronny Hadani and Anton Monk. OTFS: A New Generation of Modulation Addressing the Challenges of 5G. *CoRR*, abs/1802.02623, 2018. URL <http://arxiv.org/abs/1802.02623>.
- [2] R. Hadani, S. Rakib, M. Tsatsanis, A. Monk, A. J. Goldsmith, A. F. Molisch, and R. Calderbank. Orthogonal time frequency space modulation. *IEEE Wirel. Commun. Netw. Conf. WCNC*, pages 1–13, 2017. ISSN 15253511. doi: 10.1109/WCNC.2017.7925924.
- [3] Ronny Hadani, Shlomo Rakib, Shachar Kons, Michael Tsatsanis, Anton Monk, Christian Ibars, Jim Delfeld, Yoav Hebron, Andrea J. Goldsmith, Andreas F. Molisch, and A. Robert Calderbank. Orthogonal Time Frequency Space Modulation. *CoRR*, abs/1808.00519, 2018. URL <http://arxiv.org/abs/1808.00519>.
- [4] Linglong Dai, Bichai Wang, Yifei Yuan, Shuangfeng Han, I Chih-Lin, and Zhaocheng Wang. Non-orthogonal multiple access for 5G: solutions, challenges, opportunities, and future research trends. *IEEE Communications Magazine*, 53(9):74–81, 2015.
- [5] SM Riazul Islam, Nurilla Avazov, Octavia A Dobre, and Kyung-Sup Kwak. Power-domain non-orthogonal multiple access (NOMA) in 5G systems: Potentials and challenges. *IEEE Communications Surveys & Tutorials*, 19(2):721–742, 2017.
- [6] L. Dai, B. Wang, Z. Ding, Z. Wang, S. Chen, and L. Hanzo. A Survey of Non-Orthogonal Multiple Access for 5G. *IEEE Communications Surveys Tutorials*, 20(3):2294–2323, 2018.
- [7] H. Nikopour and H. Baligh. Sparse code multiple access. In *2013 IEEE 24th Annual International Symposium on Personal, Indoor, and Mobile Radio Communications (PIMRC)*, pages 332–336, Sept 2013. doi: 10.1109/PIMRC.2013.6666156.
- [8] F. R. Kschischang, B. J. Frey, and H. J. Loeliger. Factor graphs and the sum-product algorithm. *IEEE Transactions on Information Theory*, 47(2):498–519, 2001.
- [9] Venkatesh Khammammetti and Saif Khan Mohammed. OTFS-Based Multiple-Access in High Doppler and Delay Spread Wireless Channels. *IEEE Wirel. Commun. Lett.*, 8(2):528–531, 2019. ISSN 21622345. doi: 10.1109/LWC.2018.2878740.
- [10] G. D. Surabhi, Rose Mary Augustine, and A. Chockalingam. Multiple Access in the Delay-Doppler Domain using OTFS modulation. *CoRR*, abs/1902.03415, 2019. URL <http://arxiv.org/abs/1902.03415>.
- [11] Rose Mary Augustine and A. Chockalingam. Interleaved time-frequency multiple access using OTFS modulation. *IEEE Veh. Technol. Conf.*, 2019-Sept(1):1–5, 2019. ISSN 15502252. doi: 10.1109/VTCCFall.2019.8891404.
- [12] Zhiguo Ding, Robert Schober, Pingzhi Fan, and H. Vincent Poor. OTFS-NOMA: An Efficient Approach for Exploiting Heterogenous User Mobility Profiles. *IEEE Trans. Commun.*, 67(11):7950–7965, 2019. ISSN 15580857. doi: 10.1109/TCOMM.2019.2932934.
- [13] Aritra Chatterjee, Vivek Rangamgari, Shashank Tiwari, and Suvra Sekhar Das. Non Orthogonal Multiple Access with Orthogonal Time Frequency Space Signal Transmission. arxiv preprint, 2020.
- [14] P. Raviteja, K. T. Phan, Y. Hong, and E. Viterbo. Interference Cancellation and Iterative Detection for Orthogonal Time Frequency Space Modulation. *IEEE Transactions on Wireless Communications*, 17(10): 6501–6515, 2018.
- [15] P. Raviteja, Y. Hong, E. Viterbo, and E. Biglieri. Practical pulse-shaping waveforms for reduced-cyclic-prefix ofts. *IEEE Transactions on Vehicular Technology*, 68(1):957–961, 2019.
- [16] P. Raviteja, K. T. Phan, Q. Jin, Y. Hong, and E. Viterbo. Low-complexity iterative detection for orthogonal time frequency space modulation. In *2018 IEEE Wireless Communications and Networking Conference (WCNC)*, pages 1–6, 2018.
- [17] Shashank Tiwari, Suvra Sekhar Das, and Vivek Rangamgari. Low complexity LMMSE Receiver for OTFS. *IEEE Commun. Lett.*, 23(12):2205–2209, 2019. ISSN 15582558. doi: 10.1109/LCOMM.2019.2945564.
- [18] G. D. Surabhi and A. Chockalingam. Low-Complexity Linear Equalization for OTFS Modulation. *IEEE Commun. Lett.*, 24(2):330–334, 2020. ISSN 15582558. doi: 10.1109/LCOMM.2019.2956709.
- [19] J. Dai, K. Niu, C. Dong, and J. Lin. Improved Message Passing Algorithms for Sparse Code Multiple Access. *IEEE Transactions on Vehicular Technology*, 66(11):9986–9999, 2017.
- [20] X. Meng, Y. Wu, Y. Chen, and M. Cheng. Low Complexity Receiver for Uplink SCMA System via Expectation Propagation. In *2017 IEEE*

Wireless Communications and Networking Conference (WCNC), pages 1–5, 2017.

- [21] S. Zhang, K. Xiao, B. Xiao, Z. Chen, B. Xia, D. Chen, and S. Ma. A capacity-based codebook design method for sparse code multiple access systems. In *2016 8th International Conference on Wireless Communications Signal Processing (WCSP)*, pages 1–5, Oct 2016. doi: 10.1109/WCSP.2016.7752620.
- [22] P. Raviteja, Y. Hong, E. Viterbo, and E. Biglieri. Effective Diversity of OTFS Modulation. *IEEE Wireless Communications Letters*, 9(2): 249–253, 2020.
- [23] G. D. Surabhi, R. M. Augustine, and A. Chockalingam. On the Diversity of Uncoded OTFS Modulation in Doubly-Dispersive Channels. *IEEE Transactions on Wireless Communications*, 18(6):3049–3063, 2019.